Simulation Study of Process Latitude for Liquid Immersion Lithography

So-Yeon Baek[a], Daniel C. Cole[a], Mordechai Rothschild[b], Michael Switkes[b], Michael S.Yeung[a], and Eytan Barouch[a]

[a]Dept. Manufacturing Engineering, 15 St. Mary's Street, Boston University, Brookline, MA 02446, USA

[b]Lincoln Laboratory, Massachusetts Institute of Technology, 244 Wood Street, Lexington, MA 02420, USA

ABSTRACT

A simulation package has been developed for predicting the influence of immersion, *i.e.* the presence of a uniform liquid layer between the last objective lens and the photoresist, on optical projection lithography. This technology has engendered considerable interest in the microlithography community during the past year, as it enables the real part of the index of refraction in the image space, and thus the numerical aperture of the projection system, to be greater than unity. The simulation program described here involves a Maxwell vector solution approach, including polarization effects and arbitrary thin film multilayers. We examine here the improvement in process window afforded by immersion under a variety of conditions, including $\lambda = 193$ nm and 157 nm, annular illumination, and the use of alternating phase shift mask technology. Immersion allows printing of dense lines and spaces as small as 45 nm with acceptable process window. We also examine the effect of variations in liquid index on the process window and conclude that the index of the liquid must be known to and maintained within a few parts-per-million. This has important implications for the temperature control required in future liquid immersion projection systems.

1. INTRODUCTION

Liquid immersion lithography has risen to a promising candidate position for the micro/nanolithography technology roadmap for critical dimensions (CDs) down to perhaps 45 nm. In the last few years, several articles[1,2,3] have been written on various aspects of liquid immersion lithography. Clearly, numerous factors need to be investigated to evaluate the viability of this potentially lower cost lithography technology, including optical, fluid dynamic, and fluid property variability concerns. A simulation package, as described here, has been developed to address many of the optical issues. The package accounts for high NA imaging, via a full Maxwell vector solution approach, including polarization effects, as well as accounting for multilayers of thin film media of arbitrary complex index of refraction. This simulation capability was used to examine the process window for line and space structures, based on depth of focus (DOF), for a wide range of conditions: namely, 193 and 157 nm wavelength projection systems, numerical apertures (NA) ranging between 0.9 and 1.3, and for circular and annular illumination schemes, as well as for alternating phase shift mask structures. Liquid immersion is predicted to significantly improve printability between 45 nm and 90 nm CDs, with changes in NA required at specific CD junctions to remain on the optimal operating curve. Also examined here are the lithographic effects of changes in the index of refraction of the liquid and the constraints these impose on liquid temperature control.

The outline of our article is as follows. Section 2 describes the physical and mathematical model we implemented to predict the effects of including a uniform liquid between the last objective lens and the photoresist on the wafer. Section 3 turns to using this simulation package to ascertain the effects on printability of dense lines and spaces of various dimensions, when liquid immersion is taken into account. Section 4 considers the impact of uniform changes in real part of the index of the liquid, such as those arising from a change in temperature. Finally, we end this article in section 5 with a few concluding remarks.

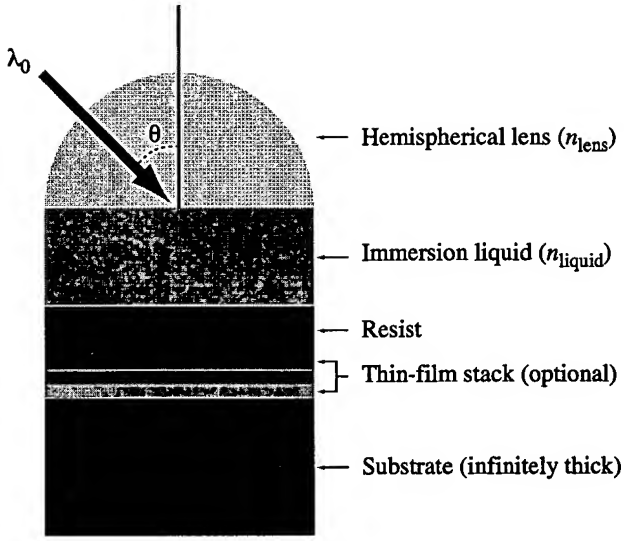

Figure 1. The physical picture of liquid immersion microlithography. The software that has been developed to simulate this arrangement can handle an arbitrary number of layers of films in the "thin-film stack", with each film described by a single complex index of refraction.

2. MODEL OF LIQUID IMMERSION LITHOGRAPHY

The model of liquid immersion lithography we made use of is shown in Fig. 1. The space between the final optical element of the projection lens (represented in Fig. 1 by a hemispherical lens) and the resist coated wafer is assumed to be filled with a high-index liquid. This effect permits exposure with incident light of large obliquity that would otherwise be totally internally reflected at the optic-air interface of a dry exposure system.[1] A light ray of wavelength λ in air entering the hemispherical lens of refractive index n_{lens} at an angle θ_{lens} contributes to an image spatial frequency $f = n_{\text{lens}} \sin\theta_{\text{lens}}/\lambda$. For a ray passing next to the rim of the lens pupil, this corresponds to a numerical aperture $\text{NA} = n_{\text{lens}} \sin\theta_{\text{lens}} = n_{\text{liquid}} \sin\theta_{\text{liquid}}$, where n_{liquid} is the liquid refractive index (assumed to be real for the present discussion) and θ_{liquid} is the propagation angle of the ray in the liquid. In order for the ray to propagate through the liquid, the numerical aperture must satisfy $\text{NA} < n_{\text{lens}}$ or n_{liquid}, whichever is less.

Suppose the Gaussian focal plane is at a distance D below the optic-liquid interface. The projection lens must provide a ray propagating in the liquid at an angle θ_{liquid} (corresponding to image spatial frequency f) with a phase shift $\Phi(f)$,

$$\begin{aligned} \Phi(f) &= -\frac{2\pi D}{\lambda} n_{\text{liquid}} \sqrt{1 - \sin^2\theta_{\text{liquid}}} \\ &= -\frac{2\pi D}{\lambda} n_{\text{liquid}} \sqrt{1 - \left(\frac{\lambda f}{n_{\text{liquid}}}\right)^2} \quad , \end{aligned} \tag{1}$$

up to an additive constant, in order for the ray to arrive at the focal plane with the correct phase. If during the exposure the liquid refractive index is actually $\tilde{n}_{\text{liquid}}$ (as a result of density fluctuation), the phase delay of the ray due to propagation from the optic-liquid interface to a plane a distance $\tilde{D}$ below the interface is $\phi(f)$,

$$\phi(f) = \frac{2\pi \tilde{D}}{\lambda} \tilde{n}_{\text{liquid}} \sqrt{1 - \left(\frac{\lambda f}{\tilde{n}_{\text{liquid}}}\right)^2} \quad . \tag{2}$$

This results in a phase error on the focal plane (where $\tilde{D} = D$) equal to $\phi(f) + \Phi(f)$,

$$\begin{aligned}\phi(f)+\Phi(f) &= \frac{2\pi D}{\lambda}\tilde{n}_{\text{liquid}}\sqrt{1-\left(\frac{\lambda f}{\tilde{n}_{\text{liquid}}}\right)^2} - \frac{2\pi D}{\lambda}n_{\text{liquid}}\sqrt{1-\left(\frac{\lambda f}{n_{\text{liquid}}}\right)^2} \\ &= \frac{2\pi D}{\lambda}(\tilde{n}_{\text{liquid}} - n_{\text{liquid}}) - \pi\lambda D\left(\frac{1}{\tilde{n}_{\text{liquid}}} - \frac{1}{n_{\text{liquid}}}\right)f^2 \\ &\quad -\frac{\pi\lambda^3 D}{4}\left(\frac{1}{\tilde{n}^3_{\text{liquid}}} - \frac{1}{n^3_{\text{liquid}}}\right)f^4 + \dots \ . \end{aligned} \tag{3}$$

Thus, fluctuation in the liquid refractive index during exposure will give rise to defocus and spherical aberrations of various orders.

The above model has been implemented in an aerial-image software for liquid immersion lithography. Vector and thin-film interference effects are taken into account[4] to allow simulation of the image intensity distribution inside the resist layer. High numerical aperture effects are also taken into account by the use of a suitable high-NA factor.[5,6]

3. DOF CALCULATIONS

Our software can calculate the light intensity throughout the entire thickness of the photoresist. However, since many resist chemistries are still under consideration for immersion lithography,[7] we concentrate on the optical effects expected by including a liquid between the last lens surface and the photoresist. Thus, the results reported here are for the light intensity just below the surface of the resist, taking into account the influence of the liquid–resist interface but not the absorbance or other properties of the bulk of the resist itself. We use the conventional aerial image threshold model procedure[8,9] to estimate the printability of such structures. We anticipate that despite the simplicity of this model, the general *trends* should still hold even when more realistic resist properties are later taken into account,

For the rest of the article, all results will be based on the light intensity calculated in the top part of the photoresist which is taken to be sufficiently thick so as to prevent reflection from the Si substrate. The various layers have the following indices: $\tilde{n} = 0.6644 + 2.04i$ for the underlying silicon, $\tilde{n} = 1.52 + 0.03i$ for the photoresist at $\lambda = 193$ nm, and $\tilde{n} = 1.4 + 0.03i$ for the photoresist at $\lambda = 157$ nm, and $\tilde{n} = 1.47$ (water) and $\tilde{n} = 1.38 + 10^{-5}i$ (perfluoropolyether) for the immersion liquids at $\lambda = 193$ nm and 157 nm, respectively. The immersion liquid thickness is taken to be 1 mm at 193 nm and 0.1 mm for 157 nm. These values reflect our best estimates for the appropriate parameters given the current state of immersion lithography[7] at 193 and 157 nm; they will undoubtedly need to be refined as the technologies develop. Still, we anticipate that the general conclusions drawn from the present simulations will remain valid.

Our initial results use contrast calculations to estimate the printability of a given aerial image. Later, we turn to exposure-defocus (ED) calculations, following conventions often discussed in B. Lin's works.[10] The contrast,

$$C = \frac{I_{\max} - I_{\min}}{I_{\max} + I_{\min}},$$

was calculated just below the surface of the photoresist. Figure 2 shows curves of contrast versus focus for four sets of equal lines and spaces with dimensions of 75, 65, 55, and 45 nm exposed with a binary mask under circular illumination with $\sigma = 0.6$. In each case, curves for NA = 1.1 and 1.3 at 193 nm and NA = 0.9 and 1.3 at 157 nm are shown. All exposures except the NA = 0.9 case are made in liquid immersion. If we take a contrast of 0.3 as an acceptable level of printability, then a reasonable estimate of the depth of focus (DOF) can be calculated from these and other similar plots, as indicated in Fig. 2(c). In Fig. 2(a), all four wavelength/NA combinations can print 75 nm L/S, with the largest DOF occurring for the NA = 1.1, $\lambda = 193$ nm case. As expected, for a given wavelength, as NA increases, one can obtain a higher level of contrast when in best focus; however, DOF is typically negatively affected.

A better perspective is shown in Figs. 3(a) and 3(b). At any given feature size, of course one wants the largest DOF in order to have as large a process window as possible. Hence, by "walking" along the upper envelope of

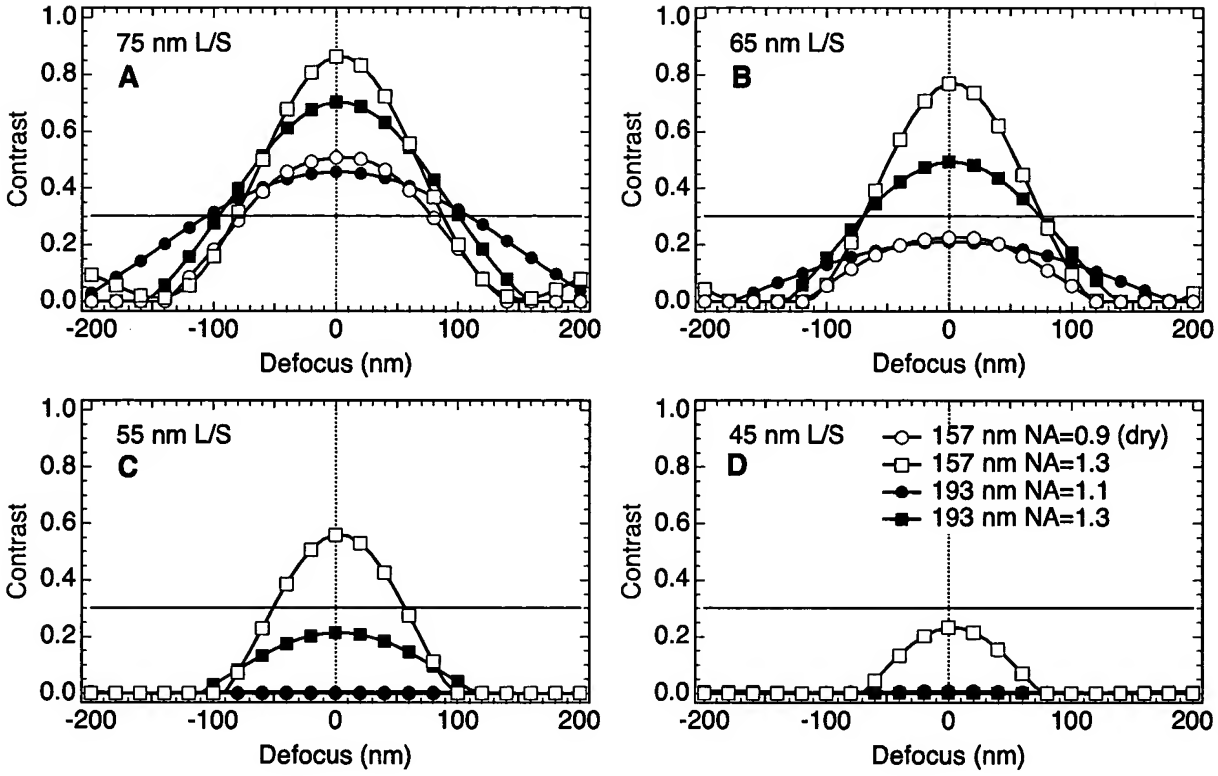

Figure 2. Contrast vs. focus for 1:1 L/S structures exposed with a binary mask and circular illumination ($\sigma = 0.6$).

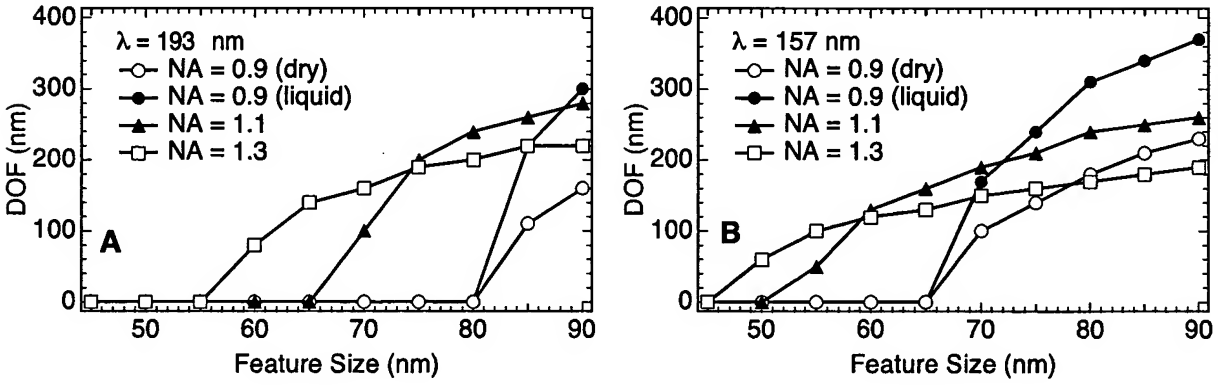

Figure 3. DOF vs. feature size with a binary mask and circular illumination for (a) $\lambda = 193$ nm; (b) $\lambda = 157$ nm, as calculated from the information in Fig. 2.

each of the curves in Figs. 3(a) and 3(b), we see roughly the desired point at each stage to best take advantage of liquid immersion capability.

Thus, liquid immersion technology offers the ability of increasing the maximum range of NA beyond unity, as well as providing a vehicle to select the most appropriate NA value for printing the features of interest, with the maximum DOF allowable. In addition, liquid immersion technology can be readily combined with other well known resolution enhancement techniques,[11] such as off-axis illumination, optical proximity corrections (OPC),

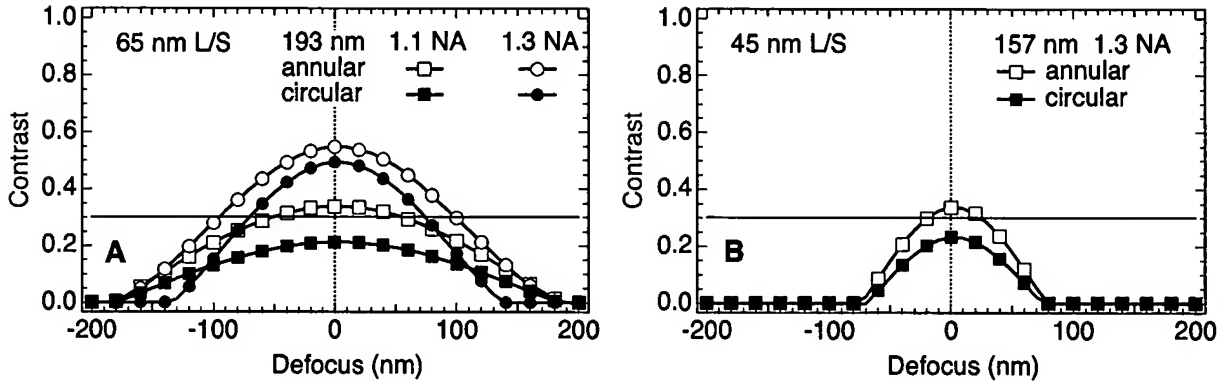

Figure 4. Comparison of contrast vs. focus for annular ($\sigma_{in} = 0.4$, $\sigma_{out} = 0.6$) and circular ($\sigma = 0.6$) illumination. (a) 65 nm L/S, $\lambda = 193$ nm; (b) 45 nm L/S, $\lambda = 157$ nm.

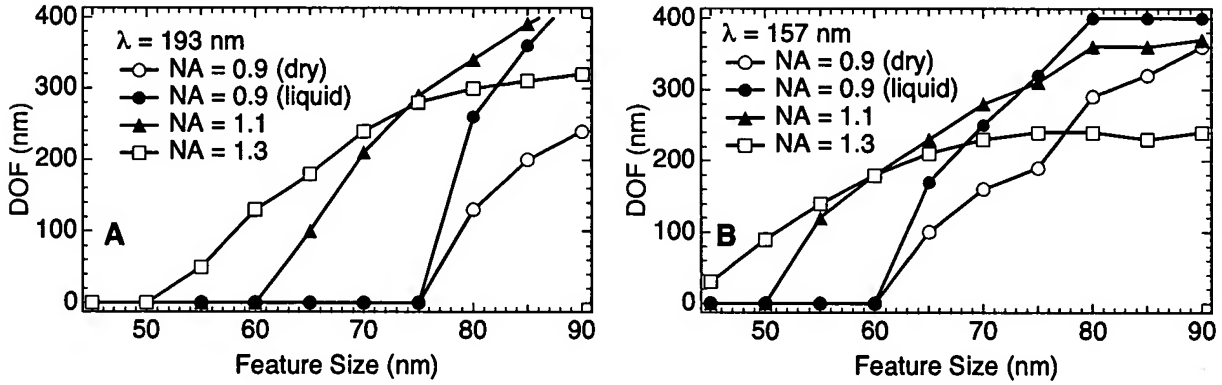

Figure 5. DOF vs. focus for annular illumination ($\sigma_{in} = 0.4$, $\sigma_{out} = 0.6$) (a) $\lambda = 193$ nm; (b) $\lambda = 157$ nm.

phase-shift mask (PSM) techniques, and focus-latitude enhancement exposure (FLEX) methods,[12] thereby pushing the limits suggested by Fig. 3.

Figures 4(a) and 4(b) provide an indication of how annular illumination, characterized by inner and outer radial parameters of 0.4 and 0.6, respectively,[6] complements immersion. In Fig. 4(a), we see that this annular partial coherence condition improves the DOF for printing 65 nm lines and spaces at NA = 1.3, $\lambda = 193$ nm, by about 30%, while at NA = 1.1, the contrast improves to about 30%, at the borderline of printability. Similarly, in Fig. 4(b), for $\lambda = 157$ nm, we see that the consideration of annular illumination, in combination with liquid immersion and an NA = 1.3, provides borderline printability for lines and spaces as small as 45 nm. Figs. 5(a) and 5(b) show the corresponding DOF for the 193 and 157 nm situations, respectively. By comparing with Fig. 3, we see that annular illumination provides a good improvement over pure circular illumination.

Similarly, if we use liquid immersion in addition to the well known method of alternating PSM, which works well for alternating features of spaces and lines of equal size, we obtain results such as those illustrated in Figs. 6 and 7. In order to take better advantage of the alternating PSM methods, a smaller partial coherence of 0.3 was used in these simulations. In Fig. 6(a), we see that with alternating PSM, a very acceptable printability should be obtained for both dry and liquid immersion at $\lambda = 193$ nm, with NA as low as 0.9, for printing 65 nm lines and spaces; this represents a considerable improvement over a binary mask with circular illumination ($\sigma = 0.6$), as in Figs. 2(b) and 3(a). Still, of course, liquid immersion provides a larger process window, even for NA=0.9. Moreover, with $\lambda = 157$ nm, as in Fig. 6(b), we see that the use of alternating PSM plus liquid immersion

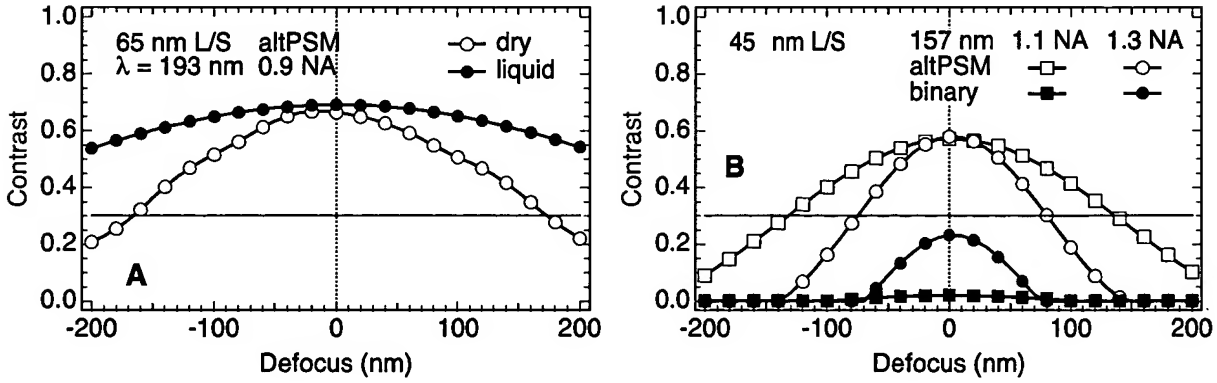

Figure 6. Comparison of contrast vs. focus for alternating PSM ($\sigma = 0.3$) and binary mask ($\sigma = 0.6$). (a) 65 nm L/S, $\lambda = 193$ nm; (b) 45 nm L/S, $\lambda = 157$ nm.

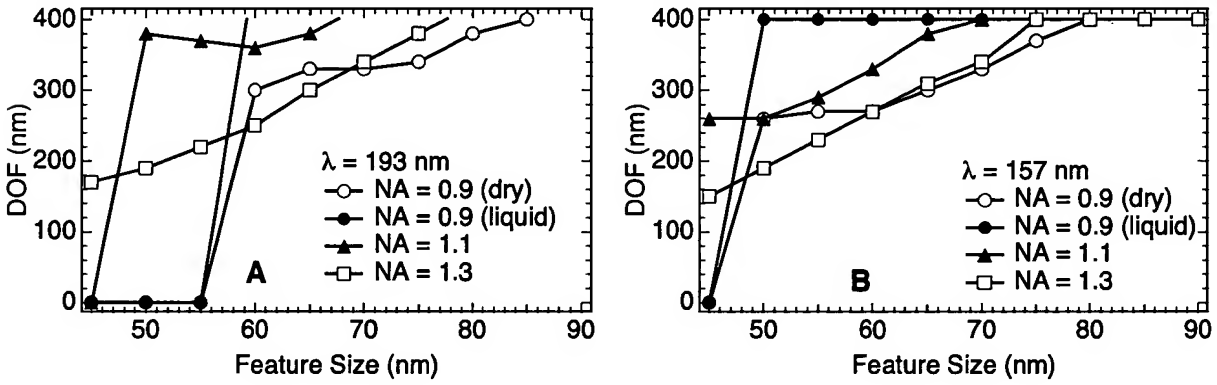

Figure 7. DOF vs. feature size for alternating PSM ($\sigma = 0.3$) (a) $\lambda = 193$ nm; (b) $\lambda = 157$ nm.

produces a very acceptable DOF for printing lines and spaces as small as 45 nm at $\lambda = 157$ nm. Finally, Figs. 7(a) and 7(b) show the DOF for various situations at $\lambda = 193$ nm and 157 nm, when the alternating PSM is used along with these very high NA applications. Tables 1, 2, and 3 summarize the data contained in Figs. 3, 6, and 7.

Circular ($\sigma = 0.6$) + Binary								
	193 nm				157 nm			
	dry	0.9	1.1	1.3	dry	0.9	1.1	1.3
45 nm	0	0	0	0	0	0	0	0
55 nm	0	0	0	0	0	0	50	100
65 nm	0	0	0	140	0	0	160	130

Table1. DOF in nm of 1:1 line/space patterns exposed with a binary mask and circular illumination ($\sigma = 0.6$).

Annular (σ = 0.4–0.6) + Binary Mask								
	193 nm				157 nm			
	dry	0.9	1.1	1.3	dry	0.9	1.1	1.3
45 nm	0	0	0	0	0	0	0	30
55 nm	0	0	0	50	0	0	120	140
65 nm	0	0	100	180	100	170	230	210

Table2. DOF in nm of 1:1 line/space patterns exposed with a binary mask and annular illumination ($\sigma_{in} = 0.4$, $\sigma_{out} = 0.6$).

Circular (σ = 0.3) + alternating PSM								
	193 nm				157 nm			
	dry	0.9	1.1	1.3	dry	0.9	1.1	1.3
45 nm	0	0	0	170	0	0	260	150
55 nm	0	0	370	220	270	400	290	230
65 nm	330	480	380	300	300	400	380	310

Table3. DOF in nm of 1:1 line/space patterns exposed with an altPSM mask and circular illumination ($\sigma = 0.3$).

The above analysis has also been generalized from simple contrast calculations, to exposure-defocus analysis, thereby enabling DOF predictions to be obtained for isolated structures, as well as more general 1D and 2D structures. Figure 8 illustrates the general idea. Figure 8(a) contains a plot of exposure versus focus for two situations, 75 nm lines and spaces exposed at 193 nm using a binary mask and circular illumination ($\sigma = 0.6$) at NA=0.9 (dry) and NA=1.1 (liquid). The DOF improvement and general increase in process window is quite evident. For any given exposure latitude, Fig. 8(a) can be used to calculate DOF, as shown in Fig. 8(b). Comparing the 75 nm point in Fig. 3(a), obtained via contrast calculations, we see excellent agreement with the 10% EL point in Fig. 8. Finally, Fig. 8(c) illustrates what happens if we push the technology using alternating PSM in addition to liquid immersion. As expected from the earlier contrast calculations, acceptable process windows look very feasible at 55 nm dimensions, with NA=1.1 and 1.3 at $\lambda = 193$ nm.

4. EFFECT OF LIQUID INDEX VARIATION

We next turn to a concern regarding liquid immersion technology that does not exist under normal conditions when the index of the vacuum or gas in the image space is very close to unity. The liquid may exhibit variations in the index as a function of space and time due to a variety of reasons, such as nonuniformity in mixing, bubbles, outgassing resulting from the chemical processes occurring in the photoresist, or, our chief concern here, nonuniformities in temperature from heating effects. We concentrate on the simplest treatment of such concerns, the effect on imaging due to a uniform change in the real part of the index of refraction of the liquid throughout the entire liquid. Clearly, other effects such as bubbles or nonuniform heating would cause problems not captured by the present simulations; we hope to be able to address such concerns in future work by making appropriate extensions to our simulation capabilities. Nevertheless, the present study at least addresses the first order concern that would need to be met to have adequate imaging capability for meeting the printability demands expected of the liquid immersion technique for microlithography.

Figure 9(a) shows how a uniform change in index throughout the liquid results in each ray being refracted differently, thereby resulting in a different image point corresponding to each point in the object space. The larger the thickness of the liquid and the larger the change in index of the liquid, the more important this consideration will be.

Figure 9(b) considers the situation of contrast versus focus for 65 nm lines and spaces, with $\lambda = 193$ nm and NA=1.3. Three curves are shown, corresponding to the situations where the change in the real part of the index of the liquid when the index varies uniformly by ± 10 ppm from its nominal value. From this, we can calculate the corresponding reduction in the DOF.

Figures 10(a), 10(b), and 10(c) examine the effect of this uniform change in index on the contrast versus focus plots previously considered. Figure 11(a) shows DOF versus the change in index for the circular illumination case, when $\lambda = 193$ nm, NA=1.3, and the liquid thickness is 1 mm. The slopes of the curves for the cases shown,

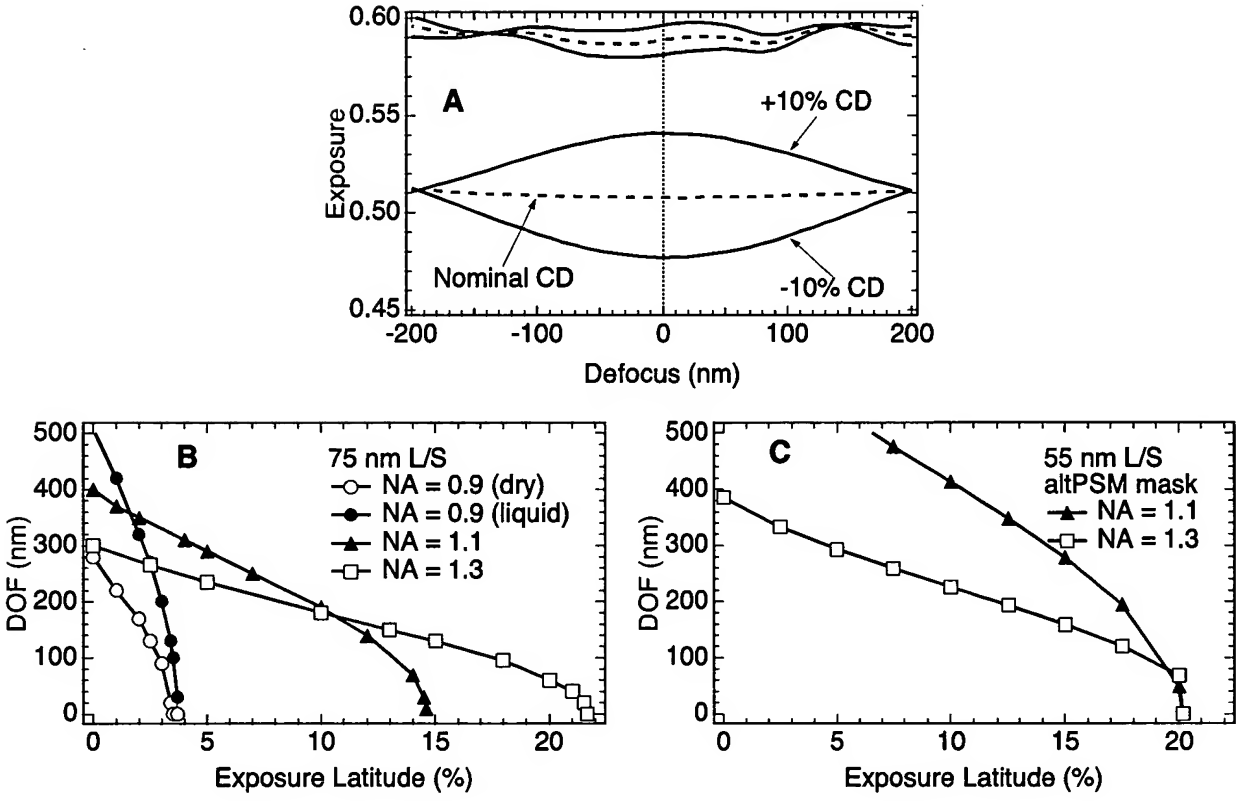

Figure 8. (a) Exposure–Defocus (ED) plot for 75 nm L/S features at $\lambda = 193$ nm with binary mask and circular illumination ($\sigma = 0.6$) at NA = 0.9 (dry exposure; top three curves) and NA = 1.1 (immersion; bottom three curves). The middle curve in each set of three represents the dose required to obtain the desired line width while the top and bottom curves represent the doses for ±10% variations in line width. The process window is considerably larger for the NA=1.1 case. (b) DOF vs. exposure latitude (EL) for 75 nm L/S, $\lambda = 193$ nm, where EL is defined here as the exposure difference between the ±10% lines, divided by the exposure at nominal printing. (c) DOF vs. EL for 55 nm L/S, $\lambda = 193$ nm, using an alternating PSM mask and $\sigma = 0.3$ illumination.

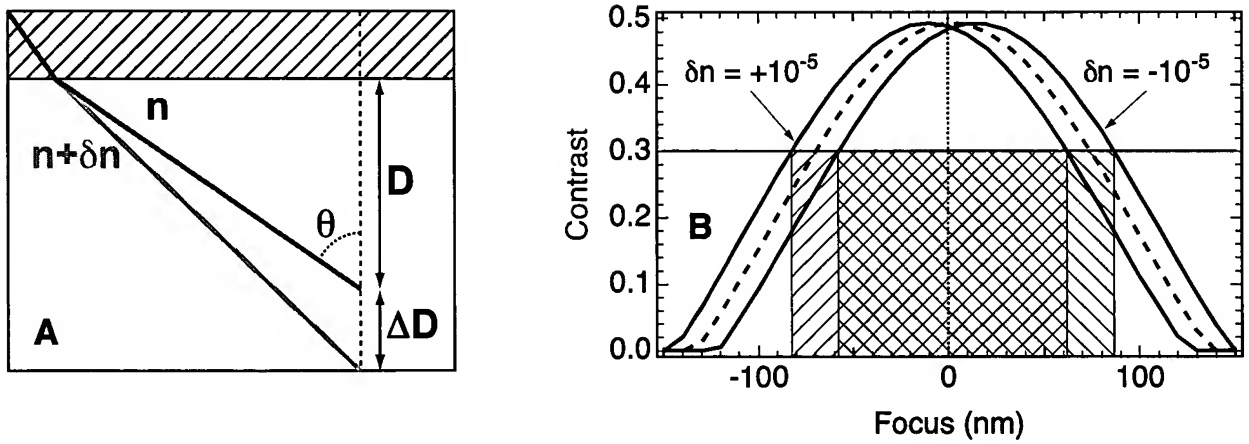

Figure 9. (a) A uniform change δn in the index of refraction of the liquid leads (to first order) to a defocus ΔD. (b) The effect of δn on the contrast for 65 nm L/S, at $\lambda = 193$ nm, NA $= 1.3$, $\sigma = 0.6$. The hatched areas represent the focus range over which contrast > 0.3 for each δn, illustrating the loss of DOF due to uncertainty in δn.

of 60, 65, 70, and 75 nm lines and spaces, are fairly similar; of course, the smaller the line/space dimension, the lower the DOF of the structure for any given δn. Figure 11(b) shows our prediction for the DOF variation as a function of the change in index, for the 65 nm situation, for all three cases of circular illumination, annular illumination, and alternating PSM. Here also, the slopes of the three curves are similar. Again, though, for any given δn, the DOF of the circular illumination is the smallest, then that of the annular, and then that of the alternating PSM.

The main conclusion to be drawn from Fig. 11 is that the liquid index must be matched to the design index to ± 10 ppm or better. If the mismatch is due only to the temperature control of the liquid, then the latter must be within ± 0.1 °C (assuming $dn/dT \approx -100$ ppm/°C for water at 193 nm).[13]

5. CONCLUDING REMARKS

The simulation package produced and described here has enabled us to examine the expected improvements in printability by using liquid immersion microlithography. Clearly, the advantages to be gained are considerable, since it appears that acceptable printability of lines and spaces with dimensions as small as 75 nm are achievable with binary masks and circular illumination at $\lambda = 193$ nm, with DOF ≈ 200 nm [Fig. 3(a)]. When combined with annular illumination, dimensions as small as about 68 nm with DOF ≈ 200 nm, still at $\lambda = 193$ nm, appear achievable. When liquid immersion is combined with an alternating PSM method, then dimensions less than 50 nm appear to be achievable with this same DOF [Fig. 7(a)]. Other resolution enhancements techniques, such as line biases, attenuated PSM, serifs, etc., should also work well since their effects are additive to those of liquid immersion.

In future work, we anticipate addressing further nonuniformity issues, as well as analyzing 2D imaging conditions, such as contact holes, islands, elbows, etc. With our present simulation package, we can analyze 2D imaging situations, as well as the problem where the index of the film varies along the optic axis, but is constant within any given plane perpendicular to the optic axis. This scenario will arise as the photoresist is heated during exposures, creating a temperature gradient in the liquid along the optic axis.[14] The more complicated issues of lateral variation of index, and of extreme changes such as those arising from bubbles in the immersion liquid, are more difficult to simulate. However, we anticipate attempting to estimate the effects of such variations in our future simulation work.

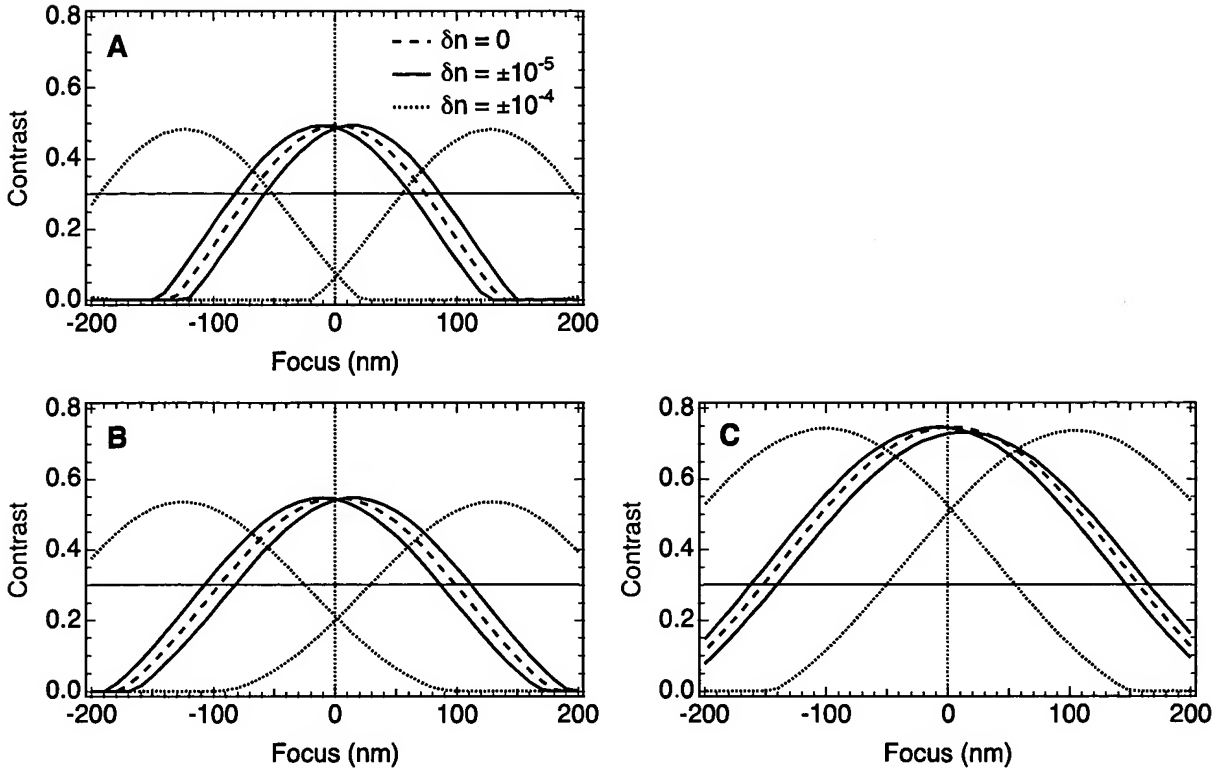

Figure 10. The effect of δn on 65 nm L/S patterns for (a) binary mask, circular illumination ($\sigma = 0.6$); (b) binary mask with annular illumination ($\sigma_{in} = 0.4$, $\sigma_{out} = 0.6$); (c) alternating PSM mask with circular illumination ($\sigma = 0.3$).

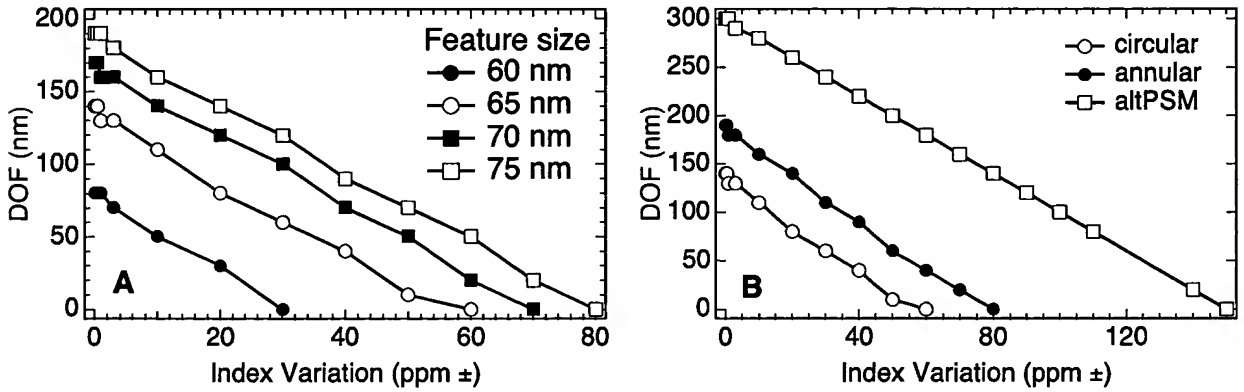

Figure 11. Sensitivity of DOF to liquid index variation at $\lambda = 193$ nm, NA = 1.3, and 1 mm liquid thickness. (a) Circular illumination ($\sigma = 0.6$) and binary mask at different L/S dimensions; (b) Different illumination and masks at 65 nm L/S.

ACKNOWLEDGMENTS

This work was performed under the Advanced Lithography Program of the Defense Advanced Research Projects Agency, under Air Force Contract F19628-00-C-0002. Opinions, interpretations, conclusions, and recommendations are those of the authors, and do not necessarily represent the view of the Department of Defense.

REFERENCES

1. M. Switkes and M. Rothschild, "Resolution enhancement of 157 nm lithography by liquid immersion," *J. Microlith., Microfab., Microsyst.* **1**, pp. 225–228, 2002.
2. J. A. Hoffnagle, W. D. Hinsberg, M. Sanchez, and F. A.Houle, "Liquid immersion deep-ultraviolet interferometric lithography", *J. Vac. Sci. Technol. B* **17**, pp. 3306–3309, 1999.
3. M. Switkes and M. Rothschild, "Immersion lithography at 157 nm", *J. Vac. Sci. Technol. B* **19**, pp. 2353–2356, 2001.
4. M. Yeung, "Modeling aerial images in two and three dimensions," *Proc. Kodak Microelectronics Seminar, Interface '85* , pp. 115–126, 1986.
5. M. S. Yeung, "Modeling high numerical aperture optical lithography," *Proc. SPIE* **922**, pp. 149–167, 1988.
6. D. C. Cole, E. Barouch, U. Hollerbach, and S. A. Orszag, "Derivation and simulation of higher numerical aperture scalar aerial images," *Jpn. J. Appl. Phys.* **31**, pp. 4110–4119, 1992.
7. M. Switkes, M. Rothschild, R. R. Kunz, R. F. Sinta, P. M. Gallagher-Wetmore, V. J. Krukonis, and K. Williams, "Immersion liquids for lithography in the deep ultraviolet," *Proc. SPIE* **5040**, 2003 (in press).
8. T. A. Brunner and R. A. Ferguson, "Approximate models for resist processing effects," *Proc. SPIE* **2726**, pp. 198–207, 1996.
9. D. C. Cole, E. Barouch, E. W. Conrad, and M. Yeung, "Using advanced simulation to aid microlithography development," *Proc. IEEE* **89**, pp. 1194–1213, 2001.
10. B. Lin and P. Young, "Full-depth optical proximity correction (FD-OPC) based on E-D forest," *Proc. SPIE* **3679**, pp. 600–606, 1999.
11. A. K.-K. Wong, *Resolution Enhancement Techniques in Optical Lithography*, vol. 47 of *Tutorial Texts in Optical Engineering*, SPIE Press, Bellingham. WA, 2001.
12. C. Spence, D. C. Cole, and B. Peck, "Using multiple focal planes to enhance depth of focus," *Proc. SPIE* **1674**, pp. 285–295, 1992.
13. P. Schiebner, J. Straub, J. M. H. Levelt Sengers, and J. S. Gallagher, "Refractive index of water and steam as function of wavelength, temperature, and density", *J. Phys. Chem. Ref. Data* **19**, pp. 677–717, 1990.
14. A. C. Wei, G. F. Nellis, A. Y. Abdo, C. Chen, R. L. Engelstad, W. A. Beckman, E. G. Lovell, M. Switkes, and M. Rothschild, "Preliminary microfluidic simulations for immersion lithography", *Proc. SPIE* **5040**, 2003 (in press).